entropy

MDPI

Article

Ecological Function Analysis and Optimization of a Recompression S-CO_2 Cycle for Gas Turbine Waste Heat Recovery

Qinglong Jin, Shaojun Xia * and Tianchao Xie

College of Power Engineering, Naval University of Engineering, Wuhan 430033, China; 18404133@masu.edu.cn (Q.J.); tianchaoxie94@gmail.com (T.X.)
* Correspondence: 2020281050888@whu.edu.cn; Tel.: +86-027-83650532

Abstract: In this paper, a recompression S-CO_2 Brayton cycle model that considers the finite-temperature difference heat transfer between the heat source and the working fluid, irreversible compression, expansion, and other irreversibility is established. First, the ecological function is analyzed. Then the mass flow rate, pressure ratio, diversion coefficient, and the heat conductance distribution ratios (HCDRs) of four heat exchangers (HEXs) are chosen as variables to optimize cycle performance, and the problem of long optimization time is solved by building a neural network prediction model. The results show that when the mass flow rate is small, the pressure ratio, the HCDRs of heater, and high temperature regenerator are the main influencing factors of the ecological function; when the mass flow rate is large, the influences of the re-compressor, the HCDRs of low temperature regenerator, and cooler on the ecological function increase; reasonable adjustment of the HCDRs of four HEXs can make the cycle performance better, but mass flow rate plays a more important role; the ecological function can be increased by 12.13%, 31.52%, 52.2%, 93.26%, and 96.99% compared with the initial design point after one-, two-, three-, four- and five-time optimizations, respectively.

Keywords: recompression S-CO_2 Brayton cycle; finite-time thermodynamics; neural network prediction; ecological function

Citation: Jin, Q.; Xia, S.; Xie, T. Ecological Function Analysis and Optimization of a Recompression S-CO_2 Cycle for Gas Turbine Waste Heat Recovery. *Entropy* **2022**, *24*, 732. https://doi.org/10.3390/e24050732

Academic Editor: Eliodoro Chiavazzo

Received: 4 May 2022
Accepted: 19 May 2022
Published: 21 May 2022

1. Introduction

A gas turbine (GT) has the advantages of a compact structure, small volume, light weight, high power density, and high thermal efficiency and is mostly used as a driving machine in surface ships and civilian ships. However, its waste heat temperature is high and has the possibility of re-utilization. Strengthening the utilization of this part of the waste heat can effectively improve the energy utilization rate [1]. The characteristics of high efficiency, better stability, economy, compactness, and simplicity make the Brayton cycle (BC) system based on supercritical carbon dioxide (S-CO_2) have broad application prospects [2–6]. Moreover, the optimal heat source temperature range of the S-CO_2 Brayton cycle (SCBC) is 450~700 °C [1], which matches the exhaust gas temperature of GT. Therefore, it is an ideal cycle for recovering the waste heat of GTs [7–11].

Sulaiman et al. [12] analyzed the performances of five different types of SCBCs integrated with solar thermal power plants, including regenerative, recompression, etc. The results show that the recompression S-CO_2 Brayton cycle (RCSCBC) has the highest thermal efficiency. Vasquez et al. [13] analyzed the regenerative, recompressed, partially cooled, and intercooled SCBC integrated with the solar receiver and obtained the optimal operating conditions through multi-objective thermodynamic optimization. Anton et al. [14] used thermodynamic modeling and analysis based on the combination of the RCSCBC with a sodium-cooled fast reactor to explore the effect of different structural layouts on the thermal

efficiency of the cycle. Alharbi et al. [15] proposed a multi-effect desalination system driven by RCSCBC waste heat, which can be used for electricity and fresh water production.

Liu et al. [16] carried out the design and analysis of the RCSCBC for ships with an output power of 40MW. The research results showed that the designed RCSCBC reached an efficiency of 45.06% at 823.15 K, which meets the design requirements and improves by 8.28% over the simple regenerative cycle. Li et al. [17] conducted a comparative study on SCBC for waste heat recovery from GTs, where selected cycles were optimized and analyzed in terms of system efficiency, etc. Khadse et al. [18] conducted a thermodynamic optimization study of the RCSCBC for waste heat recovery applications; the results show that higher pressures can result in a higher cycle power output.

Mohammadi et al. [19] proposed a combined cycle consisting of a GT cycle, an RC-SCBC, and an organic Rankine cycle. The research results showed that the cycle could effectively improve the utilization rate of heat recovery. Saeed and Kim [20] proposed a novel SCBC, which consisted of four compression processes and one expansion process, with a better ability to integrate with heat sources by comparing with the regenerative, recompression, and intercooling and regenerative cycles, and the results showed that the thermal efficiency (TEF) was comparable to that of the intercooling and regenerative cycle. Khatoon et al. [21] investigated the thermodynamic performance of an RCSCBC integrated with a direct air-cooled heat exchanger (HEX), and the research results showed that the cooling process of S-CO_2 was sensible heat transfer, and the thermophysical properties changed nonlinearly.

Although the above work has carried out analysis and research on different types of SCBCs, these studies have not considered in detail the effects of irreversible factors such as irreversible compression and irreversible expansion. The overall optimum performances of the SCBC device have not been obtained under the condition of a constant overall size of the heat exchange devices.

Finite-time thermodynamics (FTT) [22–27] realizes the cross-integration of multiple basic discipline theories including thermodynamics, heat transfer, and fluid mechanics and is an important branch of modern thermodynamic theory. FTT seeks more practical and useful performance bounds and obtains the optimal performance under limited size constraints and the optimal way to achieve the goal [28–31], whose results have important engineering value. FTT has been used in the studies of a wide variety of processes and cycles, such as the organic Rankine cycle [32–34], Carnot cycle [35], thermoelectric generator [36], Kalina cycle [37,38], and Stirling heat engine [39,40]. Combining the analysis method of FTT theory with the SCBC, on the one hand, makes up for the deficiency of the traditional pure thermodynamic analysis method in the irreversibility analysis of the SCBC. On the other hand, it can further expand the scope of application research objects of FTT, which has important theoretical and engineering significances.

In Brayton cycle research based on the "ideal gas hypothesis", Cheng and Chen [41–43] established a Brayton cycle model by considering the irreversible losses of the cyclic processes; derived the functional expressions of the cyclic power, efficiency, and ecological functions; and optimized the cycle with these performance objectives. Ust et al. [44] analyzed and studied the irreversible closed Brayton cycle with a constant-temperature heat source and the ecological performance coefficient. Kaushik et al. [45] studied the closed variable-temperature irreversible regenerative Brayton cycle model, aiming at cycle power and efficiency. Tyagi et al. [46–49] established a closed irreversible intercooling regenerative Brayton cycle model with constant-temperature and variable-temperature heat sources, respectively, and analyzed the power, efficiency, and ecological performance coefficient of the cycle.

In the FTT study of the SCBC, Na et al. [50] studied a preheating SCBC and investigated the influences of related parameters on thermal efficiency and net power output. Jin et al. [51] established an FTT model of the regenerative S-CO_2 Brayton cycle and carried out multi-objective optimization.

An RCSCBC model that considers the finite temperature difference heat transfer between the heat source and the working fluid (WF), irreversible compression, and irreversible expansion will be established in this paper. Firstly, the ecological functions are analyzed; then, under the constraint of the total HEX inventory, taking the mass flow rate, pressure ratio, diversion coefficient, and the heat conductance of each HEXs as optimization variables, performance optimization for ecological function will be performed; and the optimal design results with practical engineering application value will be given.

2. Physical Model

Figures 1 and 2 are the RCSCBC device diagram and T-s diagram, respectively. The RCSCBC device is mainly composed of the main compressor, re-compressor, low temperature regenerator (LTR), high temperature regenerator (HTR), heater, turbine, and cooler. In Figure 2, 1-2_S and 1-2 denote the ideal reversible and the actual irreversible adiabatic compression processes in the main compressor, respectively; 2-8 and 8-3 denote the heat absorption process in the LTR and HTR, respectively; 3-4 denotes the heat absorption process from the high-temperature heat reservoir; 4-5 and 4-5_S denote the actual irreversible and the ideal reversible adiabatic expansion processes, respectively; 5-6 and 6-7 denote the heat release processes in the LTR and HTR. At state point 7, the WF is divided by a flow divider, and a part of the WF enters the re-compressor; 8-7 is the actual irreversible adiabatic compression process in the re-compressor. After this, part of the WF leaves the re-compressor; it reaches the temperature of state point 8 after an isenthalpic mixing process with the WF after endothermic heating in the LTR, and 7-1 indicates the exothermic process.

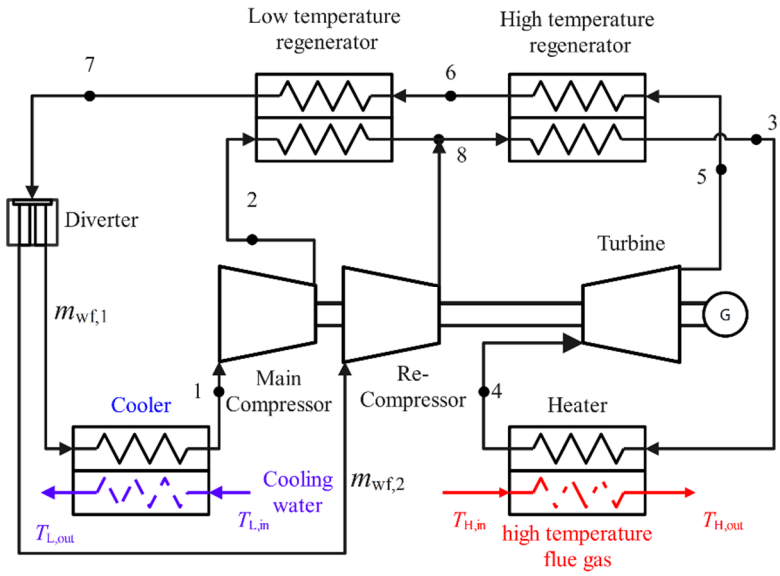

Figure 1. The device diagram of RCSCBC.

We regarded m_{wf} as the mass flow rate of the WF; $m_{wf,1}$ as the mass flow rate of WF entering the cooler through the splitter after the S-CO_2 comes out of the LTR; and $m_{wf,2}$ as the mass flow rate of WF entering the re-compressor through the splitter. Defining the ratio of $m_{wf,1}$ to m_{wf} as the diversion coefficient x_p, there is the following formula:

$$m_{wf,1} = x_p \cdot m_{wf} \tag{1}$$

$$m_{wf,2} = (1 - x_p) \cdot m_{wf} \tag{2}$$

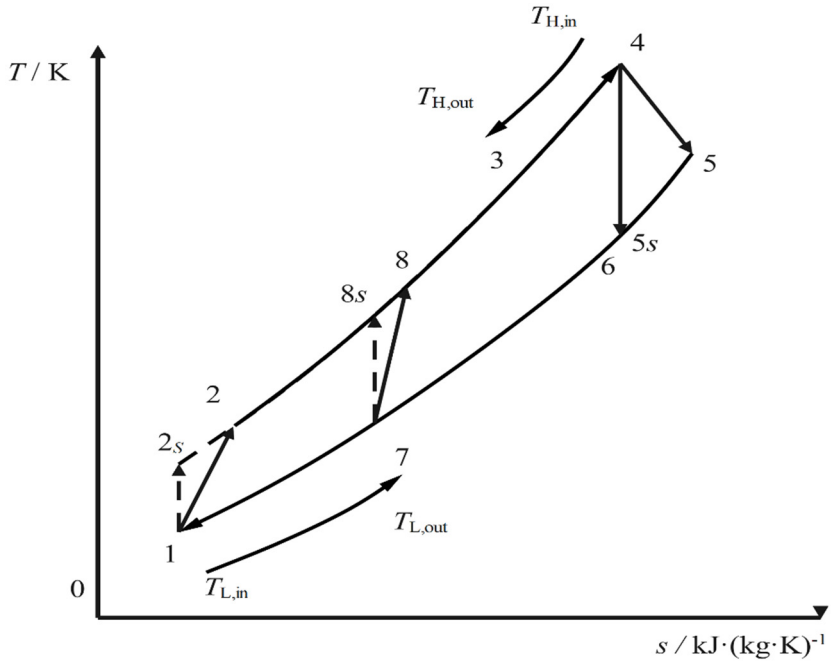

Figure 2. The *T*-*s* diagram of RCSCBC.

The efficiencies of main compressor, re-compressor, and turbine are represented by η_c, $\eta_{c,2}$, and η_t:

$$\eta_c = (h_{2s} - h_1)/(h_2 - h_1) \tag{3}$$

$$\eta_{c,2} = (h_{8s} - h_7)/(h_{8,RC} - h_7) \tag{4}$$

$$\eta_t = (h_4 - h_5)/(h_4 - h_{5s}) \tag{5}$$

where h_1, h_{2s}, $h_{8,LTR}$, $h_{8,RC}$, h_8, h_2, h_3, h_4, h_{5s}, h_5, h_6, h_{8s}, and h_7 are the specific enthalpies of the corresponding state points.

π is the pressure ratio. $T_{H,in}$, $T_{H,out}$, $T_{L,in}$, and $T_{L,out}$ are the inlet and outlet temperatures of the hot and cold source, respectively. $T_{8,LTR}$ is the temperature of the WF after being heated by LTR, $T_{8,RC}$ is the temperature of S-CO_2 after leaving the re-compressor, and T_8 is the temperature of WF after the isenthalpic mixing process; T_0 is the ambient temperature. m_H and m_L are the mass flow rates of the heat source and the cold source. The heat conductances of the heater, the cooler, the LTR, and the HTR are expressed as U_H, U_L, U_{LTR}, and U_{HTR}, respectively. According to the HEX theory, the heat absorption rate Q_H, heat release rate Q_L, and heat recovery rates Q_{LTR} and Q_{HTR} are, respectively, given by [52–56]:

$$Q_H = U_H \cdot \frac{(T_{H,in} - T_4) - (T_{H,out} - T_3)}{\ln[(T_{H,in} - T_4)/(T_{H,out} - T_3)]} = c_{p,H} \cdot m_H \cdot (T_{H,in} - T_{H,out}) \tag{6}$$

$$Q_L = U_L \cdot \frac{(T_7 - T_{L,out}) - (T_1 - T_{L,in})}{\ln[(T_7 - T_{L,out})/(T_1 - T_{L,in})]} = c_{p,L} \cdot m_L \cdot (T_{L,out} - T_{L,in}) \tag{7}$$

$$Q_{LTR} = U_{LTR} \cdot \frac{(T_6 - T_{8,LTR}) - (T_7 - T_2)}{\ln[(T_6 - T_{8,LTR})/(T_7 - T_2)]} \tag{8}$$

$$Q_{HTR} = U_{HTR} \cdot \frac{(T_5 - T_3) - (T_6 - T_8)}{\ln[(T_5 - T_3)/(T_6 - T_8)]} \tag{9}$$

From the thermal properties of the WF, Q_{H}, Q_{L}, Q_{HTR}, and Q_{LTR} are, respectively,

$$Q_{\mathrm{H}} = m_{\mathrm{wf}} \cdot (h_4 - h_3) \tag{10}$$

$$Q_{\mathrm{L}} = m_{\mathrm{wf},1} \cdot (h_7 - h_1) \tag{11}$$

$$h_8 \cdot m_{\mathrm{wf}} = h_{8,\mathrm{LTR}} \cdot m_{\mathrm{wf},1} + h_{8,\mathrm{RC}} \cdot m_{\mathrm{wf},2} \tag{12}$$

$$Q_{\mathrm{HTR}} = m_{\mathrm{wf}} \cdot (h_3 - h_8) = m_{\mathrm{wf}} \cdot (h_5 - h_6) \tag{13}$$

$$Q_{\mathrm{LTR}} = m_{\mathrm{wf},1} \cdot (h_{8,LTR} - h_2) = m_{\mathrm{wf}} \cdot (h_6 - h_7) \tag{14}$$

The total HEX inventory U_{T} is the sum of the U_{H}, U_{L}, U_{LTR}, and U_{HTR}.

$$U_{\mathrm{T}} = U_{\mathrm{LTR}} + U_{\mathrm{HTR}} + U_{\mathrm{L}} + U_{\mathrm{H}} \tag{15}$$

Define the heat conductance distribution ratio ψ. The ψ of the heater, the cooler, LTR, and HTR are expressed as $\psi_{\mathrm{H}} = U_{\mathrm{H}}/U_{\mathrm{T}}$,$\psi_{\mathrm{L}} = U_{\mathrm{L}}/U_{\mathrm{T}}$, $\psi_{\mathrm{LTR}} = U_{\mathrm{LTR}}/U_{\mathrm{T}}$, and $\psi_{\mathrm{HTR}} = U_{\mathrm{HTR}}/U_{\mathrm{T}}$, respectively. The ψ_{H}, ψ_{L}, ψ_{LTR}, and ψ_{HTR} have the following relationship:

$$\psi_{\mathrm{H}} + \psi_{\mathrm{LTR}} + \psi_{\mathrm{L}} + \psi_{\mathrm{HTR}} = 1 \tag{16}$$

For the RCSCBC, the W_{net} is the difference between the turbine power W_{t} and the compressor power consumption, W_{c}, and the compressor power consumption is the sum of the main compressor power consumption $W_{\mathrm{c},1}$ and re-compressor power consumption $W_{\mathrm{c},2}$. They are given by

$$W_{\mathrm{c},1} = m_{\mathrm{wf},1} \cdot (h_2 - h_1) \tag{17}$$

$$W_{\mathrm{c},2} = m_{\mathrm{wf},2} \cdot (h_{8,\mathrm{RC}} - h_7) \tag{18}$$

$$W_{\mathrm{c}} = W_{\mathrm{c},1} + W_{\mathrm{c},2} \tag{19}$$

$$W_{\mathrm{t}} = m_{\mathrm{wf}} \cdot (h_4 - h_5) \tag{20}$$

$$W_{\mathrm{net}} = W_{\mathrm{t}} - W_{\mathrm{c}} \tag{21}$$

The entropy production rate and ecological function E of the cycle are:

$$s_g = m_L \cdot c_{p,\mathrm{L}} \cdot \ln\left(\frac{T_{\mathrm{L,out}}}{T_{\mathrm{L,in}}}\right) - m_{\mathrm{H}} \cdot c_{p,\mathrm{H}} \cdot \ln\left(\frac{T_{\mathrm{H,in}}}{T_{\mathrm{H,out}}}\right) \tag{22}$$

$$E = W_{\mathrm{net}} - T_0 \cdot s_g \tag{23}$$

Since S-CO_2 is an actual gas, the p-V-T (V is the volume) relationship does not satisfy the ideal gas equation of state. In addition, the relationship between the specific heat capacity of S-CO_2, pressure, and temperature is very complicated, so it is impossible to obtain the explanatory formula for the temperature and specific enthalpy at each state point of the cycle. Numerical solutions for temperature and specific enthalpy can only be obtained programmatically. Under the given boundary conditions ($T_{\mathrm{H,in}}$, $T_{\mathrm{L,in}}$, U_{H}, U_{L}, U_{LTR}, U_{HTR}, η_{c}, $\eta_{\mathrm{c},2}$, and η_{t}), the nonlinear equation system composed of the Equations (1)–(16) is solved by the refpropm function and the @fsolve function, and the temperature and specific enthalpy of each state point can be obtained. The calculated specific enthalpy is further imported into Equations (17)–(23) to solve the NPO and TEF under the given boundary conditions. The specific calculation flow chart is shown in Figure 3. The cycle calculation program is written by MATLAB software, and the physical properties of S-CO_2 were calculated by REFPROP [57].

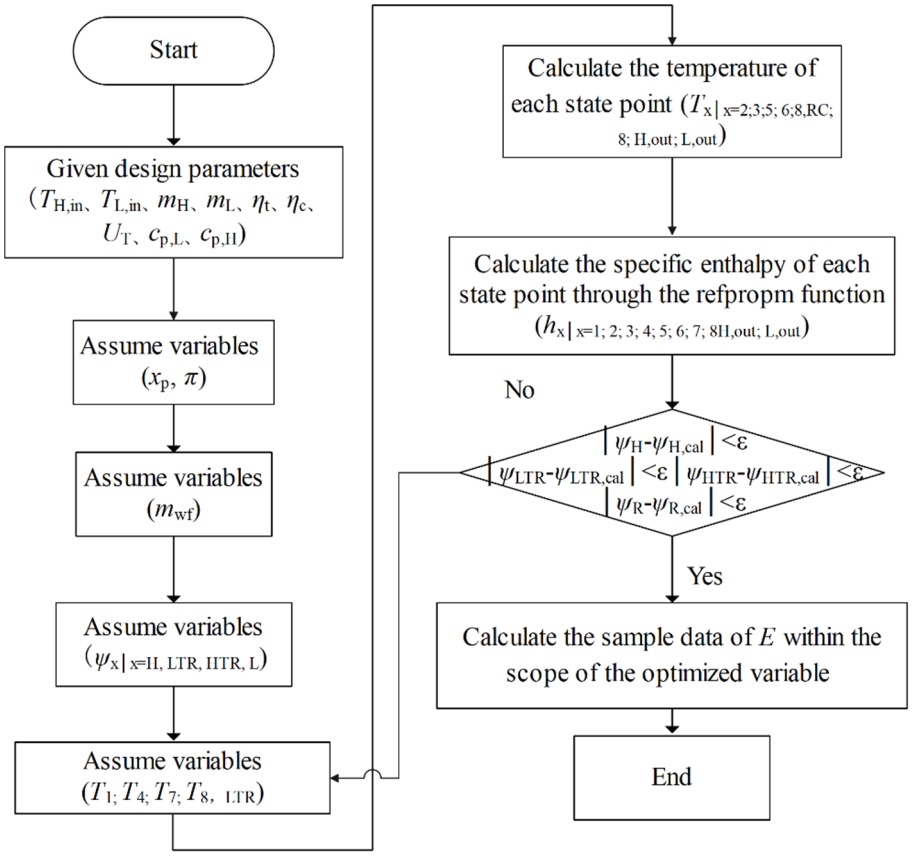

Figure 3. Calculation flow chart.

According to the Ref. [50], Table 1 gives the initial design point (IDP) parameters.

Table 1. Initial design parameters.

Parameter	Value	Parameter	Value
$T_{H,in}$	805.15 K	η_t	0.89
$T_{L,in}$	298.15 K	$\eta_{c,2}$	1.0
m_H	89.9 kg·s^{-1}	U_{HTR}	600 kW·K^{-1}
m_L	1000 kg·s^{-1}	U_H	1200 kW·K^{-1}
m_{wf}	120 kg·s^{-1}	U_{LTR}	300 kW·K^{-1}
x_p	0.8	U_L	900 kW·K^{-1}
p_{min}	7.7 MPa	$c_{p,L}$	4181.3 kJ·(kg·K)$^{-1}$
p_{max}	20 MPa	$c_{p,H}$	1103.7 kJ·(kg·K)$^{-1}$
η_c	0.89	-	-

Firstly, the cycle performance is analyzed, and the relationship between the E, x_p, and π are studied and analyzed under the conditions of different m_{wf}, η_c, and η_t. Then, with the goal of maximizing E, under the constraint that the U_T is a fixed value, the optimization will be carried out with the m_{wf}, x_p, π, ψ_H, ψ_L, ψ_{LTR}, and ψ_{HTR} as the optimization variables.

3. Results and Discussion

3.1. Ecological Function Analysis of RCSCBC

Let $\psi_{LTR} = 0.1$, $\psi_{HTR} = 0.2$, $\psi_H = 0.4$, $\psi_L = 0.3$, and $\pi = 3$, respectively. Figure 4 shows the variation trend of E with the x_p. Since the physical properties of CO_2 change drastically near the critical point, it is best to keep the T_1 above the critical point. In the case of given other parameters, the effect of the x_p on the T_1 is very obvious. Figure 4 shows the minimum x_p that can be selected according to the criterion that the T_1 must be higher than

the critical temperature under different m_{wf}. When the m_{wf} is 120 kg·s^{-1}, the selectable minimum x_p is 0.718, and when the m_{wf} is 130 kg·s^{-1}, the selectable minimum x_p is 0.76. When the m_{wf} is 140 kg·s^{-1}, the selectable minimum x_p is 0.808. Within the value range of $0.45 < x_p < 1$, the E increases first and then decreases with the x_p. After exceeding the marked minimum x_p, the E shows a decreasing trend. The x_p and m_{wf} are not just isolated variables; there is also an interaction between them. Further analysis of the regulation of the curve in Figure 4 showed that the smaller m_{wf}, the smaller the minimum x_p of the T_1 exceeding the critical temperature. This indicates that the WF split affects the temperature of each state point of the cycle, and the increase of m_{wf} can expand the selection range of the x_p.

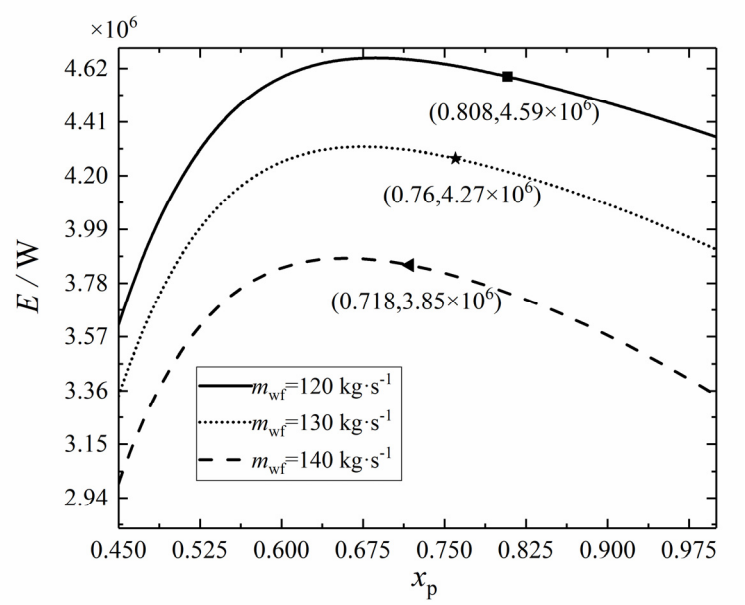

Figure 4. Effect of m_{wf} on E–x_p relation.

Let $\psi_{LTR} = 0.1$, $\psi_{HTR} = 0.2$, $\psi_H = 0.4$, $\psi_L = 0.3$, and $x_p = 0.8$, respectively. Figure 5 shows the variation trend of the E with the π under different m_{wf}s. Under the same m_{wf}, the E increases first and then decreases with the increase of the π. Additionally, there are the following characteristics, that is, with the increase of the m_{wf}, the optimal π corresponding to the maximum E gradually decreases. This is due to that the π affects the size of the net power output in both indirect and direct processes, and this influence will change with the change of m_{wf} and act on the specific value of E. In practical engineering, an appropriate π should be selected according to the corresponding environment to achieve better ecological performance.

Let $\psi_{LTR} = 0.1$, $\psi_{HTR} = 0.2$, $\psi_H = 0.4$, $\psi_L = 0.3$, and $x_p = 0.8$, respectively. Figure 6 shows the variation trend of the E with the π under different η_ts and η_cs. With the increase of η_t and η_c, the maximum E of the cycle increases, and the corresponding optimal π also increases gradually. This is due to that the values of η_t and η_c reflect the irreversibility of the expansion and compression processes. The E, as a thermodynamic index that compromises the s_g and W_{net}, can measure the irreversibility of the cycle to a certain extent; that is, there is a correlation between η_t, η_c, and the E. Therefore, the higher the η_t and η_c, the smaller the energy loss caused by the irreversibility of the cycle, and the larger the E value.

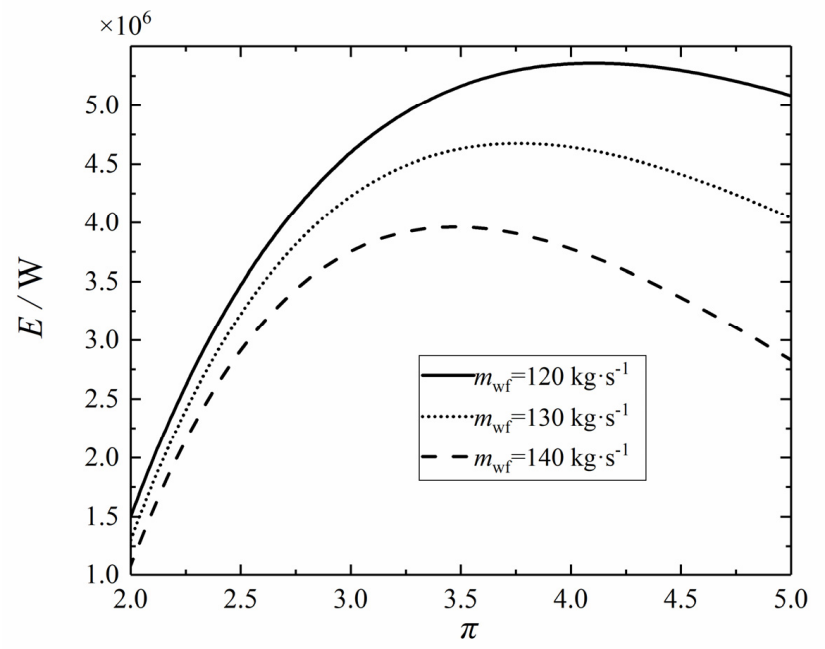

Figure 5. Effect of m_{wf} on E–π relation.

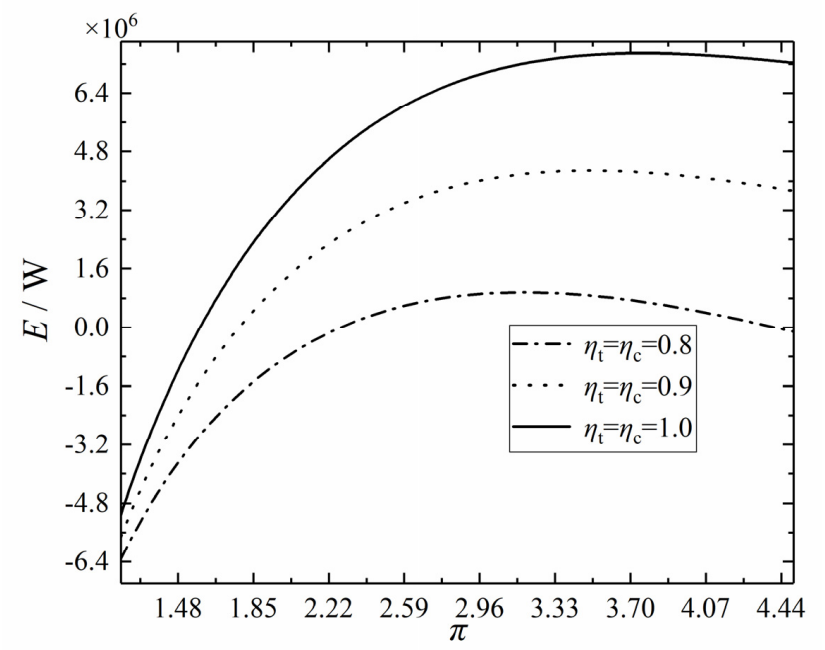

Figure 6. Effect of η_t and η_c on E–π relation.

Let ψ_{LTR} = 0.1, ψ_{HTR} = 0.2, ψ_H = 0.4, ψ_L = 0.3, and x_p = 0.8, respectively. Figure 7 shows the three-dimensional relationship between the E, m_{wf}, and π. From Figure 7, E decreases gradually with the increase of the m_{wf} and increases first and then decreases with the increase of the π. The spherical point in Figure 7 is the maximum E when the T_1 exceeds the critical temperature.

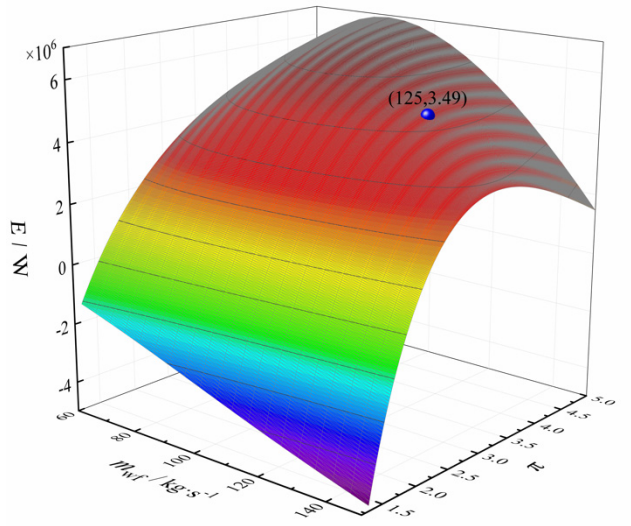

Figure 7. Three-dimensional relationship between E, m_{wf}, and π.

Let m_{wf} = 140 kg·s^{-1}, ψ_{LTR} = 0.1, ψ_{HTR} = 0.2, ψ_H = 0.4, and ψ_L = 0.3, respectively. Figure 8 shows the three-dimensional relationship between the E, x_p, and π. The spherical point in Figure 8 is the maximum E when the T_1 exceeds the critical temperature. It can be seen that the extreme points in Figures 7 and 8 are far away from the actual maximum value point. This is due to that the π, m_{wf}, and x_p have great influences on the temperature at each state point of the cycle, and the T_1 will directly affect the stability of the cycle operation. Under the combined action of these factors, the value range of the E is not the entire surface, so the optimal value that can be selected is not the actual maximum value.

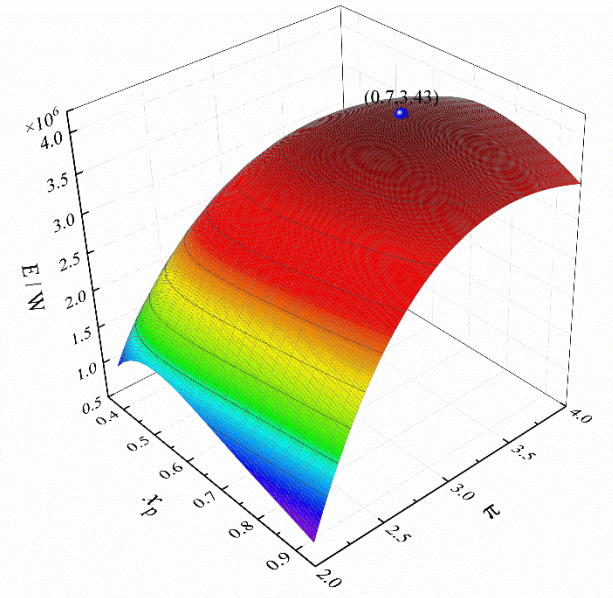

Figure 8. Three-dimensional relationship between E, x_p, and π.

Let m_{wf} = 140 kg·s^{-1}, x_p = 0.8, π = 3, and ψ_{LTR} = 0.1, respectively. Figure 9 shows the three-dimensional relationship between the E, ψ_H, and ψ_{HTR}. The spherical point in the Figure 9 is the maximum point of the E, and the ψ_H at this point is significantly higher than that of the ψ_{HTR}. It shows that under the condition of this parameter, the heater has a great influence on the E. The best performance of the cycle can be obtained by adjusting the values of the m_{wf}, π, and x_p and further optimizing the ψ_H, ψ_{HTR}, ψ_L, and ψ_{LTR}.

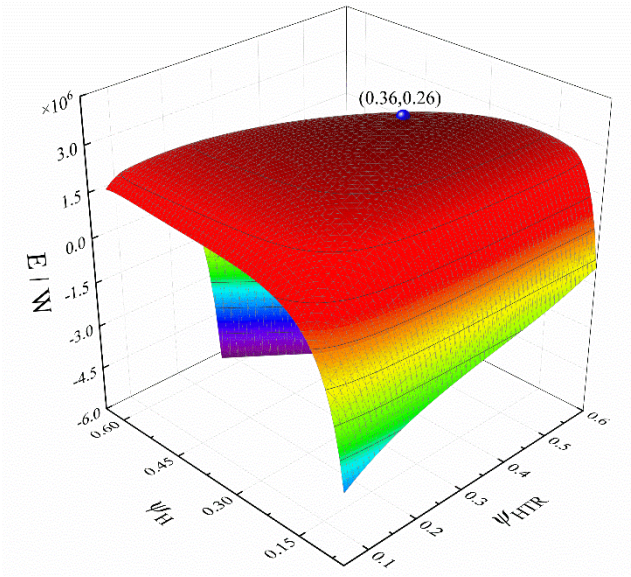

Figure 9. Three-dimensional relationship between E, ψ_H, and ψ_{HTR}.

3.2. Performance Optimization

This section will aim to maximize E under the constraint that the U_T is a fixed value. The optimization is carried out with the m_{wf}, x_p, π, ψ_H, ψ_{HTR}, and ψ_{LTR} as the optimization variables, and the specific optimization process is shown in Figure 10.

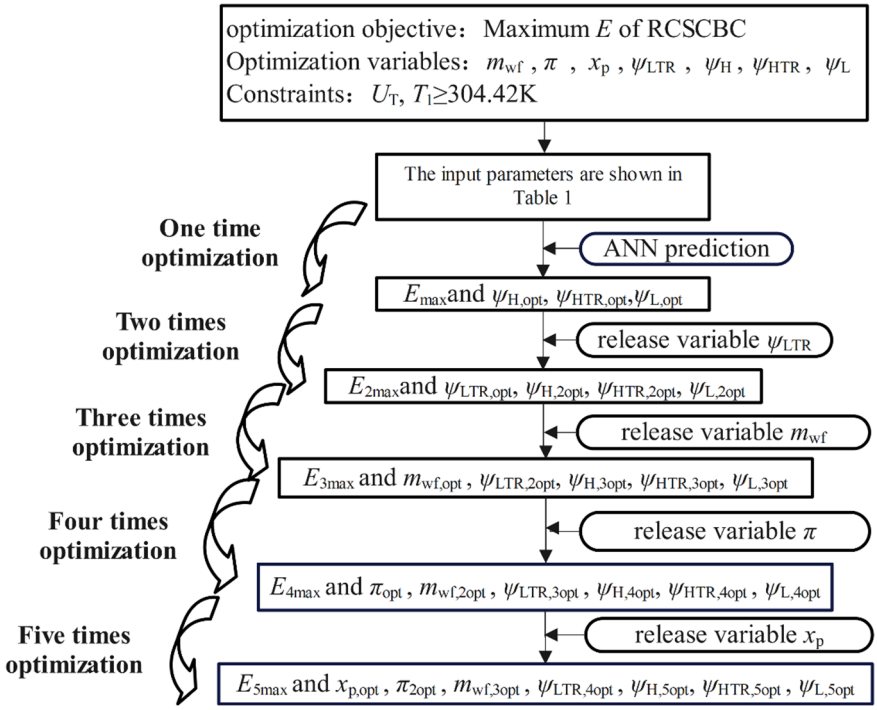

Figure 10. Optimization flow chart of RCSCBC.

The parameter constraints are shown as follows:

$$\begin{cases} 60 \le m_{\mathrm{wf}} \le 140 \left(\mathrm{kg} \cdot \mathrm{s}^{-1}\right) \\ 2 \le \pi \le 7.5 \\ 0.45 \le x_{\mathrm{p}} \le 0.9 \\ 0.01 \le \psi_{\mathrm{LTR}} \le 0.4 \\ 0.05 \le \psi_{\mathrm{HTR}} \le 0.5 \\ 0.05 \le \psi_{\mathrm{H}} \le 0.5 \end{cases} \tag{24}$$

At the same time, it is best to keep the T_1 above the critical temperature, so an additional constraint is given by

$$T_1 \ge 304.42\mathrm{K} \tag{25}$$

The performance optimization of the RCSCBC includes six optimization variables, including m_{wf}, π, x_{p} and ψ_{LTR}, ψ_{H}, ψ_{HTR}. Through the traditional solution method, there will be a problem of a large amount of calculation, and the @fsolve function is used in the calculation process to rely heavily on the initial value. The interruption of the calculation program caused by calling the REFPROP physical property library to report an error has added more difficulties to the research work. Using neural network prediction can increase the calculation speed, eliminate the need to calculate the ecological function by solving the nonlinear equation system, and get rid of the program's dependence on the calculation of the initial value. In the case of many optimization variables, neural network prediction is an effective method to simplify the calculation steps.

Therefore, this section introduces neural network prediction in the optimization of the cycle's single-objective performance.

The method of using the neural network is relatively simple. As long as the corresponding optimization variables are input into the neural network, the corresponding performance target can be obtained. A neural network can be thought of as a very convenient function. In the optimization process, it is only necessary to specify the value range of the corresponding optimization variables and then use the global search algorithm @globalsearch to call the neural network to obtain the optimal ecological function under different conditions.

Among them, constructing a neural network requires correct sample data to construct a mapping function, so its training is carried out on the basis of computational data. By constructing a neural network with a large sample amount of data, the target value of the cycle can be predicted only by entering the corresponding parameter values. Additionally, the more sample data, the closer the final trained model is to the real function. The parameter settings for training the neural network are shown in Table 2.

Table 2. Parameter settings of neural network model for the RCSCBC.

Parameter Name	E	T_1
Samples	6227	6227
Input nodes	6	6
Output	1	1
Hidden layers	2	2
Number of hidden layer nodes layer nodes	30, 15	30, 15
Hidden layer activation function	tansig, purelin	tansig, purelin
Training times	80,000	80,000
Minimum number of confirmation failures	10,000	10,000
Learning rate	120.0	120.0
Minimum training target error	1×10^{-6}	1×10^{-7}
Performance function	mse	mse

Neural networks are not just the starting point for optimization algorithms. When there are few optimization variables, the calculation process is relatively simple, but every

time one more variable is released, the calculation process becomes complicated. Therefore, a global search algorithm is used for each optimization to call the neural network for optimization.

The construction of the neural network model requires sample points, and each optimization variable is used as the input value; ecological function is the output value. The value range of each variable is shown in Equation (24). There were 6227 random sample points within the calculation range obtained by calculation, and these data are used as samples to train the neural network prediction model.

To verify the reliability of neural network prediction model, it is necessary to re-collect 36 sets of data and compare the calculated values with the predicted values. The re-collected 36 sets of test data cannot be any of the sample data. The comparison results are shown in Figure 11. According to Figure 11, neural network prediction is reliable.

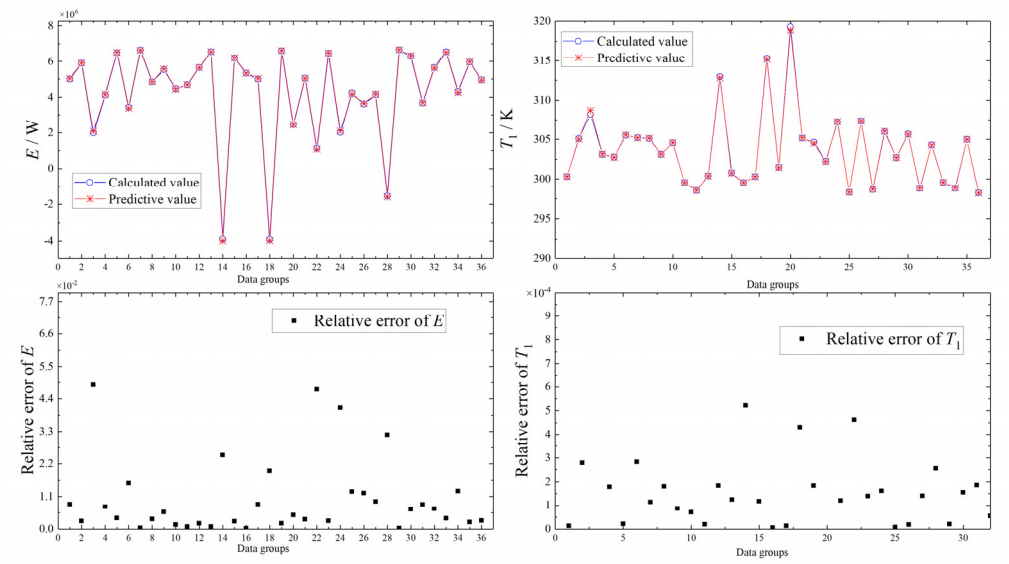

Figure 11. Comparison of predicted and calculated values of E and T_1.

Let $\pi = 3$, $x_p = 0.8$, $m_{wf} = 140$ kg·s^{-1}, and $\psi_{LTR} = 0.1$. Figure 12 shows the variation trend of E and its corresponding ψ_H and ψ_L with ψ_{HTR}. From Figure 12, with the increase of ψ_{HTR}, E first increases and then decreases, ψ_H gradually decreases, and ψ_L increases first and then decreases. When $\psi_{HTR} = 0.38$, $\psi_H = 0.25$, and $\psi_L = 0.27$, E reaches the maximum value. The reason for the difference from the optimal value given in Figure 9 comes from two aspects: one is that there is a certain error in the neural network itself, and the other is that the prediction of the neural network has volatility, but this part of the gap is within an acceptable range.

Let $\pi = 3$, $x_p = 0.8$, and $m_{wf} = 140$. Figure 13 shows the maximum E and the corresponding optimal ψ_{HTR}, ψ_H, and ψ_L under different ψ_{LTR}s. From Figure 13, with the increase of ψ_{LTR}, E first increases and then decreases, and its corresponding optimal ψ_{HTR} has a very obvious downward trend. ψ_L first increases and then decreases, but the change is small. Although ψ_H also shows a downward trend, the change is relatively small. It shows that under the premise of given other parameters, there is a relationship of mutual influence and restriction between the LTR and HTR. The reasonable distribution of ψ_{HTR} and ψ_{LTR} can make the ecological performance of the RCSCBC reach a better level.

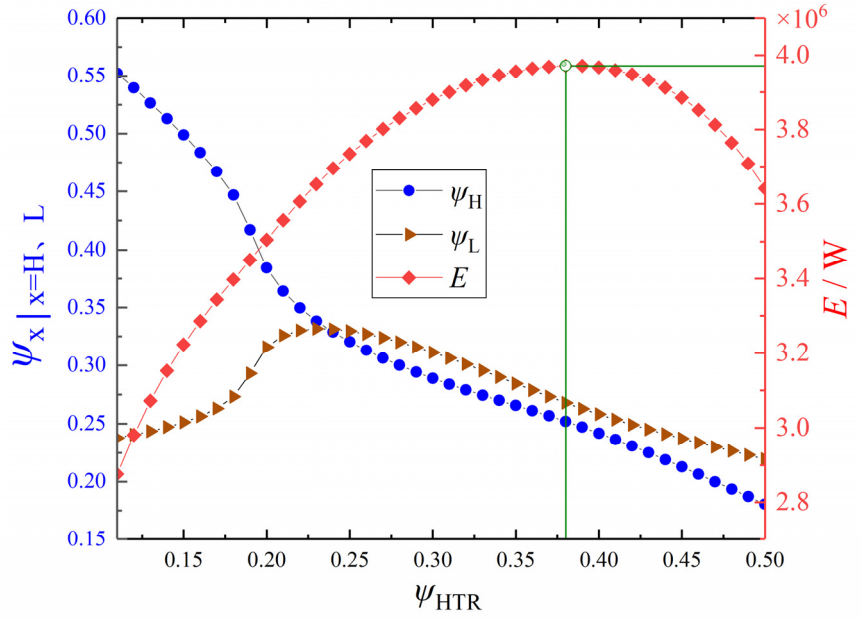

Figure 12. Profiles of E and the corresponding ψ_H and ψ_L versus ψ_{HTR}.

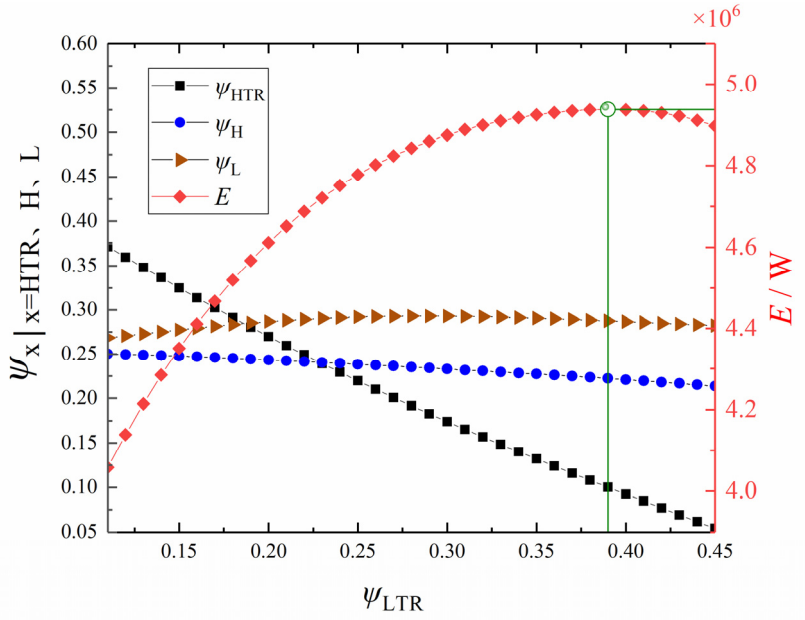

Figure 13. Profiles of E and the corresponding ψ_{HTR}, ψ_H, and ψ_L versus ψ_{LTR}.

Let $\pi = 3$ and $x_p = 0.8$. Figure 14 shows the E of the RCSCBC and its corresponding ψ_{HTR}, ψ_H, ψ_{LTR}, and ψ_L under different m_{wf}. It can be seen from Figure 14 that, given the x_p and π, the optimal value of the cyclic E first increases and then decreases with the increase of the m_{wf}. Additionally, it reaches the maximum value when the m_{wf} is in the range of 100~110 kg·s^{-1}. The changing trends of the four heat conductance distribution ratios with the m_{wf} show that ψ_H gradually decreases, ψ_L gradually increases, and ψ_{LTR} and ψ_{HTR} fluctuate up and down within a certain range. When the m_{wf} is 70, 80, and 90 kg·s^{-1}, there are inflection points in the ψ_H and ψ_{LTR}. The main reason for these inflection points is that the T_1 needs to exceed the critical temperature of carbon dioxide.

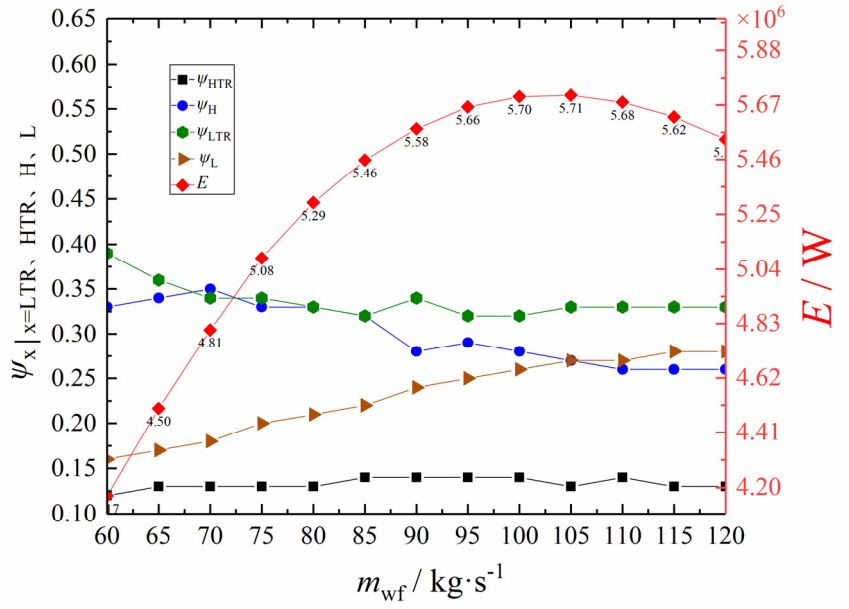

Figure 14. Profiles of E and the corresponding ψ_{PHE}, ψ_{HE}, ψ_R, and ψ_L versus m_{wf}.

Taking into account the possibility of too many variables causing the curves to be unclear in the picture, the images after four- and five-time optimizations are no longer given, and the results after four- and five-time optimizations are directly given in Table 3.

Table 3. Optimization calculation results of E based on design point.

Parameters and Objective	Initial Design Point	One-Time Optimization Result	Two-Time Optimization Result	Three-Time Optimization Result	Four-Time Optimization Result	Five-Time Optimization Result
m_{wf}/kg·s^{-1}	140	140	140	105	86.35	85.26
π	3	3	3	3	5.02	5.83
x_p	0.8	0.8	0.8	0.8	0.80	0.90
ψ_{LTR}	0.1	0.1	0.39	0.13	0.28	0.23
ψ_{HTR}	0.2	0.38	0.1	0.27	0.15	0.16
ψ_H	0.4	0.22	0.22	0.33	0.37	0.39
ψ_L	0.3	0.27	0.29	0.27	0.20	0.22
$E/\times10^6$ W	3.75	3.972	4.937	5.707	7.25	7.387
δE/%	-	5.92	31.65	52.2	93.26	96.99

Table 3 shows the results obtained by performing one-, two-, three-, four- and five-time optimizations in turn with the goal of maximizing E. It can be seen from Table 3 that after the one-time optimization, the E can be improved by 12.13% compared with the IDP. After the two-time optimization, the E can be improved by 31.52%. After the three-time optimizations, the E can be improved by 52.2%. After four-time optimization, the E can be improved by 93.26%. After five-time optimization, the E can be improved by 96.99%. From the changes of cycle parameters in the one-, two- and three-time optimizations, it can be found that when the m_{wf} is large, the ψ_{LTR} is the main factor affecting the E. After the three-time optimization, the m_{wf} corresponding to the optimal value of the E decreases, the ψ_{LTR} decreases, and the ψ_{HTR} increases. This shows that when the m_{wf} is small, the HTR is the main factor affecting the E. In addition, in the three-time optimization, the improvement of the E produces a sudden change. It shows that the heat conductance distribution ratio can make the distribution of cycle performance better, but the m_{wf} plays a much more important role.

Comparing three-, four- and five-time optimizations, it can be found that after releasing the π and m_{wf}, the parameters corresponding to the maximum E have changed significantly, which indicates that the π and m_{wf} are the main factors affecting the E.

In the five-time optimization, the x_p corresponding to the best E reaches 0.9, which is the calculation boundary of the selected parameters, which is influenced by other parameters.

Comparing the results of the five-time optimization with those of the four-time optimization, in addition to the increase of the x_p, the optimal π corresponding to the optimal E of the cycle also gradually increases, the ψ_H increases, the ψ_{HTR} increases, the ψ_{LTR} gradually decreases, and the ψ_L increases. The values of all parameters have been re-arranged and changed, which further illustrates that the relationship between the various cycle parameters is also mutual influential.

Table 4 shows the maximum E of the RCSCBC and its corresponding optimal parameters under different m_{wf}s. According to Table 4, when the m_{wf} is small, the π and x_p corresponding to the optimal value of the E are relatively large. When the m_{wf} is larger, the π and x_p are smaller. According to the definition of the x_p, the larger the x_p, the smaller m_{wf} entering the re-compressor. When the x_p is one, the RCSCBC is transformed into a RSCBC with two regenerators connected in series.

Table 4. Calculation results for the case with E_{max} as the optimization objective.

Optimization Variables							Objective	Results
m_{wf}/kg·s^{-1}	π	x_p	ψ_{LTR}	ψ_{HTR}	ψ_H	ψ_L	$E/\times 10^6$ W	δE/%
60.00	5.76	0.83	0.28	0.21	0.37	0.15	5.998	59.93
65.00	6.55	0.90	0.24	0.29	0.31	0.17	6.512	73.66
70.00	6.15	0.90	0.15	0.20	0.47	0.18	6.844	82.49
75.00	5.88	0.89	0.22	0.22	0.37	0.19	7.127	90.05
80.00	6.00	0.90	0.19	0.17	0.43	0.21	7.305	94.79
85.00	5.83	0.90	0.24	0.18	0.36	0.22	7.350	96.01
90.00	5.67	0.87	0.21	0.16	0.40	0.23	7.286	94.30
95.00	5.04	0.79	0.30	0.15	0.33	0.22	7.205	92.13
100.00	5.19	0.82	0.32	0.15	0.28	0.24	7.029	87.44
105.00	4.47	0.79	0.28	0.17	0.30	0.25	6.900	83.99
110.00	4.60	0.76	0.29	0.18	0.28	0.25	6.712	78.97
115.00	4.20	0.73	0.33	0.15	0.27	0.25	6.606	76.15
120.00	4.04	0.73	0.29	0.18	0.26	0.27	6.371	69.89
125.00	3.84	0.72	0.34	0.15	0.23	0.28	6.212	65.66
130.00	3.71	0.70	0.34	0.15	0.23	0.28	6.006	60.16
135.00	3.58	0.67	0.33	0.18	0.22	0.27	5.765	53.74

This shows that when the m_{wf} is small, the E of the RSCBC is larger and more advantageous, and when the m_{wf} is large, the E of the RCSCBC is larger, which is more advantageous than the RSCBC. Besides, the optimal π gradually decreases with the increase of m_{wf} and directly affects the ecological performance of the cycle. In actual engineering, appropriate parameters can be selected for different situations according to the data in Tables 3 and 4 to achieve the best ecological performance of the cycle.

Comparing the data in Table 4, it can be found that when the m_{wf} is 65, 75 and 100 kg·s^{-1}, there are some inflection points in the values of the x_p and π.This is due to the influence of the computational boundary, the additional constraint from the T_1, and the influence of the volatility of the neural network prediction. Considering the functionality of the RCSCBC, the x_p cannot take a value of 1, and according to Equation (24), the x_p cannot take a value greater than 0.9. Under this premise, when the m_{wf} is small, the calculation of the optimal value of the E is limited.

To sum up, when the m_{wf} is small, the π, heater, and HTR are the main factors influencing the ecological function. At a higher m_{wf}, the effects of the re-compressor, LTR, and cooler on the E increases. According to Table 4, after optimization, the E can be improved by at least 53.74% compared with the IDP.

Figure 15 shows the T_1, $T_{H,out}$, and the T_4 at each value point in Figure 14. From Figure 15, the T_1 is maintained above 304.42K but has not changed significantly. With the increase of the m_{wf}, both the $T_{H,out}$ and T_4 decrease. The temperature of each state point can provide a reference for the stable operation of the cycle and reflect the accuracy of the optimization results to a certain extent.

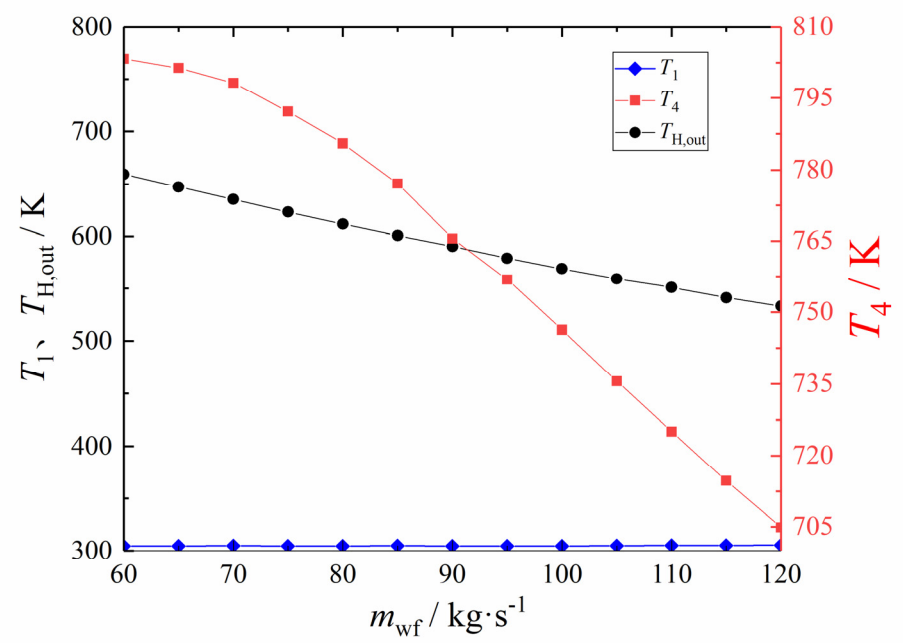

Figure 15. The variation law of T_1, T_4, and $T_{H,out}$ corresponding to E with m_{wf}.

4. Conclusions

In this paper, an FTT model of the RCSCBC was established. First, the performance analysis of the E was carried out. Then, on the premise of a certain total heat exchanger inventory, the E as optimized with the m_{wf}, π, x_p, ψ_H, ψ_{HTR}, and ψ_{LTR} as optimization variables, and the following conclusions were obtained.

(1) The values of η_t and η_c reflect the irreversibility of the expansion process and the compression process, and the E is used as a thermodynamic index for compromising entropy yield and net power. The irreversibility of the cycle can be measured to a certain extent, that is, there is a correlation between η_t, η_c, and E. The higher the η_c and η_t, the smaller the energy loss caused by the irreversibility of the cycle, and the larger the E value.

(2) When the m_{wf} is small, the π, heater and HTR are the main influencing factors on the ecological function. When the m_{wf} is large, the influences of the re-compressor, LTR, and cooler on the E increases. A reasonable adjustment of the distribution ratios of ψ_H, ψ_{HTR}, ψ_{LTR}, and ψ_L can make the cycle performance better, but m_{wf} plays a much more important role.

(3) Each cycle parameter not only affects the performance of the cycle, but also has a mutual influence relationship. The ecological function can be increased by 12.13%, 31.52%, 52.2%, 93.26%, and 96.99% compared with the IDP after one-, two-, three-, four-, and five-time optimizations.

Author Contributions: Conceptualization, Q.J. and S.X.; Funding acquisition, S.X.; Methodology, Q.J., T.X. and S.X.; Software, Q.J. and T.X.; Validation, S.X.; Writing—original draft, Q.J. and T.X.; Writing—review and editing, S.X. All authors have read and agreed to the published version of the manuscript.

Funding: This work is supported by the National Natural Science Foundation of China (Grant Nos. 51976235 and 51606218) and the Natural Science Foundation of Hubei Province (No. 2018CFB708).

Informed Consent Statement: Not applicable.

Data Availability Statement: The data that support the findings of this study are available from the corresponding author upon reasonable request.

Acknowledgments: The authors are very grateful to the reviewers for their careful, unbiased, and constructive advice, which has greatly assisted this revised manuscript.

Conflicts of Interest: The authors declare no conflict of interest.

Nomenclature

c_p	Specific heat capacity at constant pressure, $J \cdot kg^{-1} \cdot K^{-1}$
E	Ecological function, W
h	Specific enthalpy, $J \cdot kg^{-1}$
m	Mass flow rate, $kg \cdot s^{-1}$
p	Pressure, Mpa
Q	Heat transfer rate, W
s_g	Entropy production rate, $W \cdot K^{-1}$
T	Temperature, K
U	Heat conductance, $kW \cdot K^{-1}$
W	Net power output, W
x	Diversion coefficient
Greek letters	
ψ	Heat conductance distribution ratio
π	Pressure ratio
η	Efficiency
Subscripts	
c	Compressor
H	Heat source
HTR	High temperature regenerator
in	Inlet or inside
L	Cold source
LTR	Low temperature regenerator
out	Outlet or outside
RC	Re-compressor
T	Total
t	Turbine
Abbreviations	
BC	Brayton cycle
FTT	Finite-time thermodynamics
GT	Gas turbine
HCDR	Heat conductance distribution ratio
HEX	Heat exchanger
NPO	Net power output
RCSCBC	Recompression S-CO_2 Brayton cycle
S-CO_2	Supercritical Carbon-dioxide
SCBC	S-CO_2 Brayton cycle
TEF	Thermal Efficiency
WF	Working Fluid

References

1. Wright, S.A.; Parma, E.J.J.; Vernon, M.E.; Fleming, D.D.; Rochau, G.E.; Suo-Anttila, A.J.; Rashdan, A.A.; Tsvetkov, P.V. Supercritical CO_2 direct cycle Gas Fast Reactor (SC-GFR) concept. *Off. Sci. Tech. Inf. Tech. Rep.* **2011**, 91–94.
2. Luo, D.; Huang, D.G. Thermodynamic and exergoeconomic investigation of various SCO_2 Brayton cycles for next generation nuclear reactors. *Energy Convers. Manag.* **2020**, *209*, 112649. [CrossRef]

3. Espinel Blanco, E.; Valencia Ochoa, G.; Duarte Forero, J. Thermodynamic, Exergy and Environmental Impact Assessment of S-CO_2 Brayton Cycle Coupled with ORC as Bottoming Cycle. *Energies* **2020**, *13*, 2259. [CrossRef]
4. Saeed, M.; Khatoon, S.; Kim, M. Design optimization and performance analysis of a supercritical carbon dioxide recompression Brayton cycle based on the detailed models of the cycle components. *Energy Convers. Manag.* **2019**, *196*, 242–260. [CrossRef]
5. Kim, S.; Cho, Y.; Kim, M.S.; Kim, M. Characteristics and optimization of supercritical CO_2 recompression power cycle and the influence of pinch point temperature difference of recuperators. *Energy* **2018**, *147*, 1216–1226. [CrossRef]
6. Padilla, R.V.; Too, Y.C.S.; Benito, R.; Stein, W. Exergetic analysis of supercritical CO_2 Brayton cycles integrated with solar central receivers. *Appl. Energy* **2015**, *148*, 348–365. [CrossRef]
7. Jokar, M.A.; Ahmadi, M.H.; Sharifpur, M.; Meyer, J.P.; Pourfayaz, F.; Ming, T. Thermodynamic evaluation and multi-objective optimization of molten carbonate fuel cell-supercritical CO_2 Brayton cycle hybrid system. *Energy Convers. Manag.* **2017**, *153*, 538–556. [CrossRef]
8. Wang, S.; Li, B. Thermodynamic Analysis and Optimization of a Novel Power-Water Cogeneration System for Waste Heat Recovery of Gas Turbine. *Entropy* **2021**, *23*, 1656. [CrossRef]
9. Montes, M.J.; Linares, J.I.; Barbero, R.; Moratilla, B.Y. Optimization of a New Design of Molten Salt-to-CO_2 Heat Exchanger Using Exergy Destruction Minimization. *Entropy* **2020**, *22*, 883. [CrossRef]
10. Rogalev, N.; Rogalev, A.; Kindra, V.; Komarov, I.; Zlyvko, O. Structural and Parametric Optimization of S–CO_2 Nuclear Power Plants. *Entropy* **2021**, *23*, 1079. [CrossRef]
11. Siddiqui, M.E.; Almitani, K.H. Proposal and Thermodynamic Assessment of S-CO_2 Brayton Cycle Layout for Improved Heat Recovery. *Entropy* **2020**, *22*, 305. [CrossRef] [PubMed]
12. Al-Sulaiman, F.A.; Atif, M. Performance comparison of different supercritical carbon dioxide Brayton cycles integrated with a solar power tower. *Energy* **2015**, *82*, 61–71. [CrossRef]
13. Vasquez, P.R.; Too, Y.C.S.; Benito, R.; McNaughton, R.; Stein, W. Multi-objective thermodynamic optimisation of supercritical CO_2 Brayton cycles integrated with solar central receivers. *Int. J. Sustain. Energy* **2018**, *37*, 1–20. [CrossRef]
14. Anton, M.; James, J.S. Investigation of alternative layouts for the supercritical carbon dioxide Brayton cycle for a sodiumcooled fast reactor. *Nucl. Eng. Des.* **2009**, *239*, 1362–1371.
15. Alharbi, S.; Elsayed, M.L.; Chow, L.C. Exergoeconomic analysis and optimization of an integrated system of supercritical CO_2 Brayton cycle and multi-effect desalination. *Energy* **2020**, *197*, 117225. [CrossRef]
16. Liu, Z.; Ju, Y.P.; Zhang, C.H. Thermodynamic Design of A Supercritical CO_2 Brayton Cycle for 40 MW Shipboard Application. *Compress. Blower Fan Technol.* **2019**, *61*, 67–71.
17. Li, B.; Wang, S.; Wang, K.; Song, L. Comparative investigation on the supercritical carbon dioxide power cycle for waste heat recovery of gas turbine. *Energy Convers. Manag.* **2021**, *228*, 113670. [CrossRef]
18. Khadse, A.; Blanchette, L.; Kapat, J.; Vasu, S.; Hossain, J.; Donazzolo, A. Optimization of Supercritical CO_2 Brayton Cycle for Simple Cycle Gas Turbines Exhaust Heat Recovery Using Genetic Algorithm. *J. Energy Resour. Technol.* **2018**, *140*, 71601. [CrossRef]
19. Mohammadi, K.; Ellingwood, K.; Powell, K. A novel triple power cycle featuring a gas turbine cycle with supercritical carbon dioxide and organic Rankine cycles: Thermoeconomic analysis and optimization. *Energy Convers. Manag.* **2020**, *220*, 113123. [CrossRef]
20. Saeed, M.; Kim, M. A newly proposed supercritical carbon dioxide Brayton cycle configuration to enhance energy sources integration capability. *Energy* **2022**, *239*, 121868. [CrossRef]
21. Khatoon, S.; Ishaque, S.; Kim, M. Modeling and analysis of air-cooled heat exchanger integrated with supercritical carbon dioxide recompression Brayton cycle. *Energy Convers. Manag.* **2021**, *232*, 113895. [CrossRef]
22. Bejan, A. General criterion for rating heat-exchanger performance. *Int. J. Heat Mass Transf.* **1978**, *21*, 655–658. [CrossRef]
23. Andresen, B.; Berry, R.S.; Nitzan, A.; Salamon, P. Thermodynamics in finite time. I. The step-Carnot cycle. *Phys. Rev. A* **1977**, *15*, 2086–2093. [CrossRef]
24. Bejan, A. Entropy generation minimization: The new thermodynamics of finite-size devices and finite-time processes. *J. Appl. Phys.* **1996**, *79*, 1191–1218. [CrossRef]
25. Hoffmann, K.H.; Burzler, J.; Fischer, A.; Schaller, M.; Schubert, S. Optimal Process Paths for Endoreversible Systems. *J. Non-Equil. Ther.* **2003**, *28*, 233–268. [CrossRef]
26. Andresen, B.; Salamon, P.; Berry, R.S. Thermodynamics in finite time. *Phys. Today* **2008**, *37*, 62–70. [CrossRef]
27. Chen, L.; Wu, C.; Sun, F. Finite Time Thermodynamic Optimization or Entropy Generation Minimization of Energy Systems. *J. Non-Equil. Ther.* **2000**, *24*, 327–359. [CrossRef]
28. Hoffmann, K.H. An introduction to endoreversible thermodynamics. *Atti Accad. Peloritana Pericolanti* **2008**, *86*, 1–18.
29. Ge, Y.; Chen, L.; Sun, F. Progress in Finite Time Thermodynamic Studies for Internal Combustion Engine Cycles. *Entropy* **2016**, *18*, 139. [CrossRef]
30. Andresen, B. Current trends in finite-time thermodynamics. *Angew. Chem.* **2015**, *50*, 2690–2704. [CrossRef]
31. Açıkkalp, E. Exergetic sustainability evaluation of irreversible Carnot refrigerator. *Phys. A Stat. Mech. Appl.* **2015**, *436*, 311–320. [CrossRef]
32. Feng, H.J.; Chen, W.J.; Chen, L.G.; Tang, W. Power and efficiency optimizations of an irreversible regenerative organic Rankine cycle. *Energy Convers. Manag.* **2020**, *220*, 113079. [CrossRef]

33. Wang, L.; Bu, X.; Li, H. Multi-objective optimization and off-design evaluation of organic rankine cycle (ORC) for low-grade waste heat recovery. *Energy* **2020**, *203*, 117809. [CrossRef]
34. Zerom, M.S.; Gonca, G. Multi-criteria performance analysis of dual miller cycle—Organic rankine cycle combined power plant. *Energy Convers. Manag.* **2020**, *221*, 113121. [CrossRef]
35. Ahmadi, M.H.; Ahmadi, M.A.; Sadatsakkak, S.A. Thermodynamic analysis and performance optimization of irreversible Carnot refrigerator by using multi-objective evolutionary algorithms (MOEAs). *Renew. Sustain. Energy Rev.* **2015**, *51*, 1055–1070. [CrossRef]
36. Elghool, A.; Basrawi, F.; Ibrahim, H.; Ibrahim, T.K.; Ishak, M.; Yusof, T.M.; Bagaber, S.A. Enhancing the performance of a thermo-electric generator through multi-objective optimisation of heat pipes-heat sink under natural convection. *Energy Convers. Manag.* **2020**, *209*, 112626. [CrossRef]
37. Zhou, C.; Zhuang, Y.; Zhang, L.; Liu, L.; Shen, S. A novel pinch-based method for process integration and optimization of Kalina cycle. *Energy Convers. Manag.* **2020**, *209*, 112630. [CrossRef]
38. Feng, H.; Qin, W.; Chen, L.; Cai, C.; Ge, Y.; Xia, S. Power output, thermal efficiency and exergy-based ecological performance optimizations of an irreversible KCS-34 coupled to variable temperature heat reservoirs. *Energy Convers. Manag.* **2020**, *205*, 112424. [CrossRef]
39. Ahmadi, M.H.; Ahmadi, M.A.; Maleki, A.; Pourfayaz, F.; Bidi, M.; Acikkalp, E. Exergetic sustainability evaluation and multi-objective optimization of performance of an irreversible nanoscale Stirling refrigeration cycle operating with Maxwell–Boltzmann gas. *Renew. Sustain. Energy Rev.* **2017**, *78*, 80–92. [CrossRef]
40. Ahmadi, M.H.; Ahmadi, M.A.; Pourfayaz, F.; Hosseinzade, H.; Acıkkalp, E.; Tlili, I.; Feidt, M. Designing a powered combined Otto and Stirling cycle power plant through multi-objective optimization approach. *Renew. Sustain. Energy Rev.* **2016**, *62*, 585–595. [CrossRef]
41. Cheng, C.; Chen, C. Power optimization of an irreversible Brayton heat engine. *Energy Source* **1997**, *19*, 461–474. [CrossRef]
42. Cheng, C.Y.; Chen, C.K. Efficiency Optimizations of an Irreversible Brayton Heat Engine. *J. Energy Resour. Technol.* **1998**, *120*, 143–148. [CrossRef]
43. Cheng, C.Y.; Chen, C.K. Ecological optimization of an irreversible Brayton heat engine. *J. Phys. D Appl. Phys.* **1999**, *32*, 350. [CrossRef]
44. Ust, Y.; Sahin, B.; Kodal, A.; Akcay, I.H. Ecological coefficient of performance analysis and optimization of an irreversible regenerative-Brayton heat engine. *Appl. Energy* **2006**, *83*, 558–572. [CrossRef]
45. Kaushik, S.C.; Tyagi, S.K. Finite time thermodynamic analysis of an irreversible regenerative closed cycle brayton heat engine. *Int. J. Sol. Energy* **2002**, *22*, 141–151. [CrossRef]
46. Tyagi, S.K.; Chen, J.; Kaushik, S.C. The performance characteristics of an irreversible regenerative intercooled Brayton cycle at maximum thermoeconomic function. *Int. J. Ambient. Energy* **2005**, *26*, 155–168. [CrossRef]
47. Tyagi, S.K.; Kaushik, S.C. Ecological optimisation of an irreversible regenerative intercooled Brayton heat engine with direct heat loss. *Int. J. Ambient. Energy* **2005**, *26*, 81–92. [CrossRef]
48. Tyagi, S.K.; Wang, S.W.; Chen, G.M.; Han, X.H.; Kaushik, S.C. Optimal criteria for different parameters of an irreversible regenerative intercooled Brayton cycle under maximum power and maximum ecological COP conditions. *Int. J. Ambient. Energy* **2005**, *26*, 155–168. [CrossRef]
49. Tyagi, S.K. Effects of intercooling on the performance of an irreversible regenerative Brayton cycle. *Int. J. Sol. Energy* **2009**, *28*, 231–245.
50. Na, S.I.; Kim, M.S.; Baik, Y.J.; Kim, M. Optimal allocation of heat exchangers in a Supercritical carbon dioxide power cycle for waste heat recovery. *Energy Convers. Manag.* **2019**, *199*, 112002. [CrossRef]
51. Jin, Q.; Xia, S.; Li, P.; Xie, T. Multi-objective performance optimization of regenerative S-CO_2 Brayton cycle based on neural network prediction. *Energy Convers. Manag. X* **2022**, *14*, 100203. [CrossRef]
52. Chen, L.G.; Sun, F.R.; Wu, C. Theoretical analysis of the performance of a regenerative closed Brayton cycle with internal irreversibilities. *Energy Convers. Manag.* **1997**, *38*, 871–877. [CrossRef]
53. Chen, L.G.; Wang, J.H.; Sun, F.R. Power density optimisation of endoreversible closed intercooled regenerated Brayton cycle. *J. Energy Inst.* **2007**, *80*, 105–109. [CrossRef]
54. Chen, L.G.; Wang, J.H.; Sun, F.R.; Al, E. Power density optimization of an irreversible variable-temperature heat reservoir closed intercooled regenerated Brayton cycle. *Int. J. Ambient. Energy* **2009**, *30*, 9–26. [CrossRef]
55. Chen, L.G.; Zheng, J.L.; Sun, F.R.; Wu, C. Power, power density and efficiency optimization for a closed cycle helium turbine nuclear power plant. *Energy Convers. Manag.* **2003**, *44*, 2393–2401. [CrossRef]
56. Chen, L.G.; Sun, F.R.; Wu, C. Optimum Heat Conductance Distribution for Power Optimization of a Regenerated Closed Brayton Cycle. *Int. J. Green Energy* **2005**, *2*, 243–258. [CrossRef]
57. Span, R.; Wagner, W. A New Equation of State for Carbon Dioxide Covering the Fluid Region from the Triple-Point Temperature to 1100 K at Pressures up to 800 MPa. *J. Phys. Chem. Ref. Data* **1996**, *25*, 1509–1596. [CrossRef]